AD-A232 573

REPORT DOCUMENTATION PAGE

Public reporting burden for this collection of information is estimated to average 1 hour per response, including the time for reviewing instructions, searching existing data sources, gathering and maintaining the data needed, and completing and reviewing the collection of information. Send comments regarding this burden estimate or any other aspect of this collection of information, including suggestions for reducing this burden, to Washington Headquarters Services, Directorate for Information Operations and Reports, 1215 Jefferson Davis Highway, Suite 1204, Arlington, VA 22202-4302, and to the Office of Management and Budget, Paperwork Reduction Project (0704-0188), Washington, DC 20503.

1. AGENCY USE ONLY (Leave blank)	2. REPORT DATE February 1991	3. REPORT TYPE AND DATES COVERED Journal article**

4. TITLE AND SUBTITLE
Edge-Connected, Crossed-Electrode Array for Two-Dimensional Projection and Beamforming**

5. FUNDING NUMBERS

Work Unit #59-0593

Assession #DN880-326

6. AUTHOR(S)
Harvey C. Schau*

7. PERFORMING ORGANIZATION NAME(S) AND ADDRESS(ES)
Materials Branch, Underwater Sound Reference Detachment,
Naval Research Laboratory
P.O. Box 568337
Orlando, FL 32856-8337

8. PERFORMING ORGANIZATION REPORT NUMBER

DTIC

9. SPONSORING/MONITORING AGENCY NAME(S) AND ADDRESS(ES)
Office of Naval Technology

10. SPONSORING/MONITORING AGENCY REPORT NUMBER

11. SUPPLEMENTARY NOTES *Author is no longer employed at NRL-USRD.
**Published in IEEE Transactions on Signal Processing Vol. 39 (2) 289-297 (Feb 91)

12a. DISTRIBUTION/AVAILABILITY STATEMENT

Approved for public release; distribution unlimited

12b. DISTRIBUTION CODE

13. ABSTRACT (Maximum 200 words)

A new geometry for array construction is discussed which employs two sets of orthogonal striped electrodes. While obtaining N^2 intersecting points in a two-dimensional structure, only 2N control points are required. Thus, N^2 active elements are controlled with 2N degrees of freedom which both simplifies implementation and data handling. This gain in simplicity is traded off against reduced performance when employed as a projector and increased signal processing when employed in beamforming mode. It is shown that no performance is lost in beamforming if the process is carried out in a two-step process. The limitations of the crossed-electrode geometry are discussed and a theory is presented for operation as a projector and a receiver.

14. SUBJECT TERMS Crossed-electrode array;
Two-dimensional Beamforming;   Wave Vector Filter
Two-dimensional Projection;

15. NUMBER OF PAGES
10

16. PRICE CODE

17. SECURITY CLASSIFICATION OF REPORT	18. SECURITY CLASSIFICATION OF THIS PAGE	19. SECURITY CLASSIFICATION OF ABSTRACT	20. LIMITATION OF ABSTRACT
Unclassified	Unclassified	SAR	SAR

GENERAL INSTRUCTIONS FOR COMPLETING SF 298

The Report Documentation Page (RDP) is used in announcing and cataloging reports. It is important that this information be consistent with the rest of the report, particularly the cover and title page. Instructions for filling in each block of the form follow. It is important to *stay within the lines* to meet *optical scanning requirements*.

Block 1. Agency Use Only *(Leave blank)*.

Block 2. Report Date. Full publication date including day, month, and year, if available (e.g. 1 Jan 88). Must cite at least the year.

Block 3. Type of Report and Dates Covered. State whether report is interim, final, etc. If applicable, enter inclusive report dates (e.g. 10 Jun 87 - 30 Jun 88).

Block 4. Title and Subtitle. A title is taken from the part of the report that provides the most meaningful and complete information. When a report is prepared in more than one volume, repeat the primary title, add volume number, and include subtitle for the specific volume. On classified documents enter the title classification in parentheses.

Block 5. Funding Numbers. To include contract and grant numbers; may include program element number(s), project number(s), task number(s), and work unit number(s). Use the following labels:

C	-	Contract	PR	- Project
G	-	Grant	TA	- Task
PE	-	Program Element	WU	- Work Unit Accession No.

Block 6. Author(s). Name(s) of person(s) responsible for writing the report, performing the research, or credited with the content of the report. If editor or compiler, this should follow the name(s).

Block 7. Performing Organization Name(s) and Address(es). Self-explanatory.

Block 8. Performing Organization Report Number. Enter the unique alphanumeric report number(s) assigned by the organization performing the report.

Block 9. Sponsoring/Monitoring Agency Name(s) and Address(es). Self-explanatory.

Block 10. Sponsoring/Monitoring Agency Report Number. *(If known)*

Block 11. Supplementary Notes. Enter information not included elsewhere such as: Prepared in cooperation with...; Trans. of...; To be published in.... When a report is revised, include a statement whether the new report supersedes or supplements the older report.

Block 12a. Distribution/Availability Statement. Denotes public availability or limitations. Cite any availability to the public. Enter additional limitations or special markings in all capitals (e.g. NOFORN, REL, ITAR).

> **DOD** - See DoDD 5230.24, "Distribution Statements on Technical Documents."
> **DOE** - See authorities.
> **NASA** - See Handbook NHB 2200.2.
> **NTIS** - Leave blank.

Block 12b. Distribution Code.

> **DOD** - Leave blank.
> **DOE** - Enter DOE distribution categories from the Standard Distribution for Unclassified Scientific and Technical Reports.
> **NASA** - Leave blank.
> **NTIS** - Leave blank.

Block 13. Abstract. Include a brief *(Maximum 200 words)* factual summary of the most significant information contained in the report.

Block 14. Subject Terms. Keywords or phrases identifying major subjects in the report.

Block 15. Number of Pages. Enter the total number of pages.

Block 16. Price Code. Enter appropriate price code *(NTIS only)*.

Blocks 17. - 19. Security Classifications. Self-explanatory. Enter U.S. Security Classification in accordance with U.S. Security Regulations (i.e., UNCLASSIFIED). If form contains classified information, stamp classification on the top and bottom of the page.

Block 20. Limitation of Abstract. This block must be completed to assign a limitation to the abstract. Enter either UL (unlimited) or SAR (same as report). An entry in this block is necessary if the abstract is to be limited. If blank, the abstract is assumed to be unlimited.

Edge-Connected, Crossed-Electrode Array for

Two-Dimensional Projection

and Beamforming

Harvey C. Schau

91 3 01   009

Edge-Connected, Crossed-Electrode Array for Two-Dimensional Projection and Beamforming

Harvey C. Schau. *Member. IEEE*

Abstract—A new geometry for array construction is discussed which employs two sets of orthogonal striped electrodes. While obtaining N^2 intersecting points in a two-dimensional structure, only $2N$ control points are required. Thus, N^2 active elements are controlled with $2N$ degrees of freedom which both simplifies implementation and data handling. This gain in simplicity is traded off against reduced performance when employed as a projector and increased signal processing when employed in beamforming mode. It is shown that no performance is lost in beamforming if the process is carried out in a two-step process. The limitations of the crossed-electrode geometry are discussed and a theory is presented for operation as a projector and a receiver.

INTRODUCTION

THE purpose of this paper is the introduction of a new geometry for planar structures which allows simpler implementation and construction while trading off higher signal processing costs and possible reduced performance (the term planar is not strictly necessary although most applications are concerned with planar devices). Since two-dimensional structures are important in acoustic arrays and optical imaging devices, the structure described here has applications which cover a wide variety of technical areas. In this analysis, we will give the basic operation principles of the geometry and leave detailed analysis of specific applications to a forum where the physics of each may be dealt with in detail.

The generic physical description of our device is shown in Fig. 1(b). It is assumed that an active material (acoustical or optical) is placed between two electrodes as shown. By applying a voltage, the device is able to act as a projector of acoustical or optical energy or, left in a passive state, it may create a voltage by the action of a field (acoustic or optical) impinging upon it. Obviously, this is a simplification to any real device, but for the purposes of describing a new geometrical implementation for a two-dimensional array, it is sufficient. The active material could be a piezoelectric material for acoustical applications (polyvinylidene fluoride PVDF), a nematic liquid crystal or light emitting diode material (GaAs) for optical projection applications or a Si-based optical imaging device. There exists a plethora of materials and applications which we will not discuss; however, we do make the realistic assumption that all electrodes are transparent to the type of field (acoustic or optical) under consideration.

Fig. 1 shows a two-dimensional structure which is typical of the planar arrays under consideration. In a conventional imple-
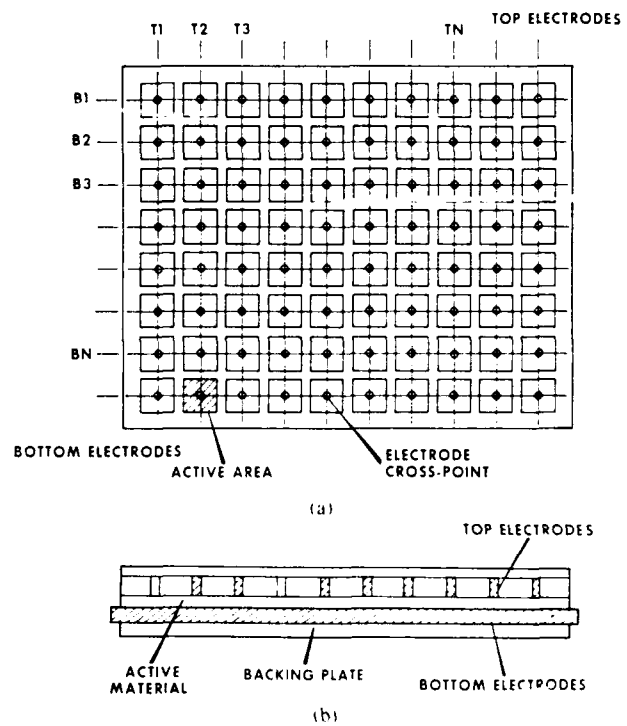
Fig. 1. Two-dimensional crossed-electrode array. (a) Top view. (b) cut-away side view.

mentation, the active element is sandwiched between electrodes and each may be addressed individually either by a random address scheme where each pair of electrodes leads is available, or through a parallel-to-serial conversion such as in charge coupled devices (CCD). The problems of individual access of each element are myriad: large numbers of connections, large numbers of wires, greater potential for failure, etc. The heat loss along conducting wires in cooled detectors, and the inability to package a random array were two major motivations for the development of the parallel-to-serial conversion devices such as CCD's. The basic problem is that for an $N \times N$ device. N^2 elements must be addressed. The contribution of this paper is to suggest another type of structure, that of crossed electroded strips as shown in Fig. 1. Here the device has one set of electrode strips on top of the active material, and another orthogonal set on the bottom. This leaves N^2 intersection points while resulting in only $2N$ electrodes which are brought out to the edge. Obviously, an array with $2N$ degrees of freedom (DOF) will not function as efficiently as one with N^2, but if one considers the savings for a device with, for example, 10^3 elements

per side (2×10^3 versus 10^6) this loss of performance may be acceptable.

We will analyze this structure through reciprocity, i.e., as a projector first, later as a receiver for beamforming. We will neglect crosstalk which can be present in a device with either $2N$ or N^2 DOF. Given the results shown in subsequent sections on projection and beamforming, a decision can be made on the feasibility of employing a crossed-electrode edge-coupled array in specific acoustical or optical applications.

TWO-DIMENSIONAL EDGE-CONTROLLED ARRAY

Consider Fig. 1. The device pictured has an active material sandwiched between two sets of electrodes. The top set consists of a number N of strips, while the bottom has a similar pattern rotated $90°$.

By applying a voltage to each top electrode and each bottom electrode, a potential difference at the intersection of the ith bottom and jth top electrodes of ($B_i - T_j$) is formed. Electric field strength may be approximated as this potential difference divided by the electrode separation, and the emitted field will be assumed to be the product of the electric field and a constant which describes the material. In acoustics, this constant would be the piezoelectric d constant, whereas in optics it is the dielectric ϵ constant for liquid crystals or another conversion factor which relates light intensity to voltage for devices such as a biased light emitting diodes operated over their linear regions. The figure indicates the active area to be the spatial intersection of two rectangular electrodes. Actually, fringing of the fields will cause a response pattern to fall off more gradually than the perfectly rectangular shape shown. This structure is both physically realizable and controllable within current signal processing technology.

Questions which remain are what types of fields may be created by such a device, and the possibility of employing such a device as a receiver. Additional investigations must center around control stability, possible implementation problems, and methodology for possible improvements.

THEORY—PROJECTION

The field generated from each active area is linearly proportional to the electric field, which is nearly proportional to the potential difference at that location. Then the potential difference at any intersection point where the ith bottom electrode crosses the jth top electrode may be written as M_{ij}

$$M_{ij} = B_i - T_j \qquad (1)$$

where B, T are the top and bottom electrode voltages for the ith row and jth column. Notice that while the number of active areas of an $N \times N$ structure device has N^2 (DOF), the edge-interconnected structure reduces this to $2N$ DOF thus limiting the types of patterns which may be represented. It is expected that the desired two-dimensional spatial fields have finite correlation lengths and times, which will reduce the number of DOF required to describe their spatial and temporal behavior. An alternate position from which to view this is to consider the description an isotropic field (isotropic assumption is not necessary but simplifies the discussion) in terms of its Karhunen-Loeve (K-L) expansion [1]-[4]. The diagonalization of the autocorrelation (expanding in terms of its eigenfunctions) matrix typically shows that the autocorrelation matrix is not of full rank and the number of eigenvalues which exceed some arbitrarily

small number is less than the dimensionality of the autocorrelation matrix.

Whereas for two-dimensional fields without correlation, each eigenvalue provides the same amount of information for describing the field in terms of an expansion of eigenvectors, with finite correlation each eigenvalue provides proportionally more information than the next smaller one, so that truncation of the expansion after a few terms yields an accurate description [5]. Thus practically speaking, the required number of DOF to expand a function which has finite correlation properties, is less than the dimensionality of the problem if the expansion is allowed to have a finite but small mean-squared error. Since even full expansions will have some variance from the original function due to noise, this limited DOF expansion may not be an overwhelming constraint.

The problem of approximating N^2 independent potential differences by $2N$ edge voltages may be represented in matrix form as

$$AV = W \qquad (2)$$

where V is the array of edge voltages, bottom voltage first, followed by top voltages. For N channels it takes the form (see Fig. 1).

$$V = \begin{bmatrix} B_1 \\ B_2 \\ \vdots \\ B_N \\ T_1 \\ T_2 \\ \vdots \\ T_N \end{bmatrix} \quad 2N \text{ elements.} \qquad (3)$$

The array W is the array of two-dimensional potential differences ordered row-wise (the array W is proportional to the desired two-dimensional field on the surface of the array)

$$W = \begin{bmatrix} M_{11} \\ M_{12} \\ \vdots \\ M_{1N} \\ M_{21} \\ \vdots \\ M_{NN} \end{bmatrix} \quad N^2 \text{ elements} \qquad (4)$$

and the matrix A has the form

$$A = \begin{bmatrix} 1 & 0 & 0 & 0 & \cdots & -1 & 0 & 0 & 0 & \cdots \\ 1 & 0 & 0 & 0 & \cdots & 0 & -1 & 0 & 0 & \cdots \\ \vdots & & & & & & & & & \\ 0 & 1 & 0 & 0 & \cdots & -1 & 0 & 0 & 0 & \cdots \\ \vdots & & & & & & & & & \\ 0 & 0 & & \cdots & 1 & 0 & 0 & 0 & 0 & \cdots & -1 \end{bmatrix} \quad N^2 \text{ elements.} \qquad (5)$$

Since A has more rows than columns the generalized inverse is

$$A^{\#} = (A'A)^{-1}A' \text{ (overdetermined case)} \tag{6}$$

and it is well known that the solution to (2) takes the general form (if the original equation is consistent) [7]

$$V = A^{\#}W + (I - A^{\#}A)Z \tag{7}$$

where $A^{\#}$ is the Penrose–Moore inverse and Z is arbitrary. We choose a solution of the form

$$V = A^{\#}W \tag{8}$$

which given the form for $A^{\#}$ in (6) for the overdetermined case, the solution (8) is best in a least squares sense.

Since the quantities of interest are voltage differences between the rows and columns, it is convenient to introduce a normalization which fixes the absolute voltage. This can be achieved in a variety of ways, one which is sufficiently general is to write

$$\sum_{i=1}^{N} B_i + \sum_{i=1}^{N} T_i = C \tag{9}$$

i.e., fix the sum of all edge voltages at some arbitrary constant C. Other forms of normalization can be found from this approach. This adds a constraint equation to (2) and changes the form of A and W. Writing the augmented equation in the form

$$BV = T$$

$$B = \begin{bmatrix} 1 & 1 & 1 & 1 & 1 & 1 & \cdots \\ & & A & & & \end{bmatrix} \qquad T = \begin{bmatrix} C \\ W \end{bmatrix} \tag{10}$$

where A and W are given by (5) and (4), respectively. Equation (10) has solution

$$V = B^{\#}T; \qquad B^{\#} = (B^{T}B)^{-1}B^{T}. \tag{11}$$

In this formulation

$$(B^{T}B) = \begin{bmatrix} \alpha & 0 \\ 0 & \alpha \end{bmatrix}$$

$$\alpha = \begin{bmatrix} N+1 & 1 & 1 & 1 & \cdots \\ 1 & N+1 & 1 & 1 & \cdots \\ \vdots & & & & \end{bmatrix} \tag{12}$$

and 0 is the $(N \times N)$ null matrix.

The inverse is easily found to be

$$(B^{T}B)^{-1} = \frac{1}{2N^{2}} \begin{bmatrix} \beta & 0 \\ 0 & \beta \end{bmatrix}$$

$$\beta = \begin{bmatrix} 2N-1 & -1 & -1 & \cdots \\ -1 & 2N-1 & -1 & \cdots \\ \vdots & & & \end{bmatrix} \tag{13}$$

which may be written as

$$(B^{T}B)^{-1} = \frac{1}{N}I + \frac{1}{2N^{2}}S$$

$$S = \begin{bmatrix} -1 & 0 \\ 0 & -1 \end{bmatrix} \tag{14}$$

where 1 is the $(N \times N)$ matrix consisting of all ones, 0 the $(N \times N)$ null matrix. The pseudoinverse is then written as

$$B^{\#} = (B^{T}B)^{-1}B^{T} = \left| \frac{1}{N}I + \frac{1}{2N^{2}}S \right| B'$$

$$= \frac{B^{T}}{N} + \frac{1}{2N^{2}}Q \tag{15}$$

$$Q = \begin{bmatrix} -N & -1 & -1 & -1 & \cdots \\ -N & -1 & -1 & -1 & \cdots \\ -N & & & & \\ \vdots & & & & \\ -N & -1 & -1 & -1 & \\ & & & & \\ -N & 1 & 1 & 1 & \\ -N & 1 & 1 & 1 & \\ \vdots & & & & \end{bmatrix}. \tag{16}$$

The final solution may be written in terms of the nonaugmented operators as

$$V = \left| \frac{1}{N}A^{T} + \frac{1}{2N^{2}}G \right| W + K \tag{17}$$

where

$$G = \begin{bmatrix} -1 & -1 & -1 & -1 & \cdots \\ \vdots & & & & \\ -1 & -1 & -1 & -1 & \cdots \\ 1 & 1 & 1 & 1 & \cdots \\ \vdots & & & \vdots & \end{bmatrix} \tag{18}$$

and

$$K = \frac{C}{2N} \begin{bmatrix} 1 \\ 1 \\ 1 \\ 1 \\ \vdots \end{bmatrix}. \tag{19}$$

The action of each matrix in (17) is easily seen if one analyzes the eigenvectors of $AA^{\#}$, where $A^{\#} = (1/N)A' + (1/2N^{2})G$. This matrix has eigenvectors which are analogous to the impulse response of the structure. The eigenvectors are unity row or column matrices which would result if a voltage were imposed on one of the edge connections. If the resulting two-dimensional pattern were analyzed by discrete Fourier transform, the first term in (17) correctly predicts the Fourier components at the price of overestimating the dc component of the two-dimensional pattern. The second term corrects the two-dimensional dc component by adjusting the overall gains of the electrode voltages row-wise or column-wise as a whole. The final

term biases the row and column voltages to obtain the desired range as initially constrained by the constant C.

Of greater importance, any two-dimensional pattern must be expandable in terms of the sum of these basis vectors which are functions of the row coordinate or the column coordinate. Analysis of the basis functions indicates that traveling harmonic disturbances moving parallel to the row or column are possible thus allowing the device to reproduce specific monochromatic spatial frequency convective waves, however, isolated impulses are not capable of accurate reproduction without the same type of error found in liquid crystal displays [8].

EXAMPLES

Consider the example of a 3×3 device in Fig. 2 where the desired spatial pattern is shown. Pattern W_1 is the sum of an eigenvector expansion. Voltages applied at each electrode are given by $A^\# W$, application of these voltages results in the original desired pattern as shown. This is guaranteed since W was given as an expansion of eigenfunctions of $AA^\#$. Note that the voltages $V = A^\# W$ are not unique (the last term in (17)) and alternate voltages shown will also reproduce the pattern (different K in (17)). Notice that the latter voltages are specified by integer values. Consider W_2, a pattern which cannot be generated by an eigenvector expansion. Voltages are again shown by $A^\# W$, however, this time the resulting pattern $AA^\# W$ has been altered. This is expected since all output will have to be an eigenvector of $AA^\#$ whether the input was or not.

Figs. 3 and 4 display two examples for a 10×10 device with 100 two-dimensional elements. At the top of each figure are desired two-dimensional fields. These patterns are typical of shading which might be required in producing a uniform convective pressure field from a planar array, in coherent optical spatial filtering employing liquid crystals or similar devices, or optical apodization of an optical system by tailoring illumination through devices such as LED's.

It can be seen that the two-dimensional field produced is in both cases a close replica of the desired field. Fig. 4 has more spatial structure than Fig. 3 and hence the replicated field has higher error in reproducing it. This is a general property of this type of replication, the more structure or high spatial frequency information the field contains (particularly in regions away from the spatial frequency axis if one visualizes performing a two-dimensional discrete Fourier transform on the desired two-dimensional pattern), the greater the error may be in reproducing it.

BEAMFORMING, TRACKING

The geometry under discussion can also be employed as a receiver, and this is perhaps the application of greater interest in both acoustics (beamforming) and optics (imaging and target tracking). Of particular importance in acoustics is the use of this geometry as a wave vector filter in rejection of turbulent boundary layer noise in favor of low frequency radiative acoustic signals, and the measurement of low frequency evanescent turbulent pressure fields [9]-[12]. In optics, it will be shown that the geometry has advantages in that tracking may be accomplished with high resolution with considerably less complication. By way of demonstration of the use of the device and how it differs in application from conventional devices, while retaining the ability to achieve the same results, we reformulate the beamforming problem for the crossed-electrode geometry and contrast it to the case of independent sensing elements.
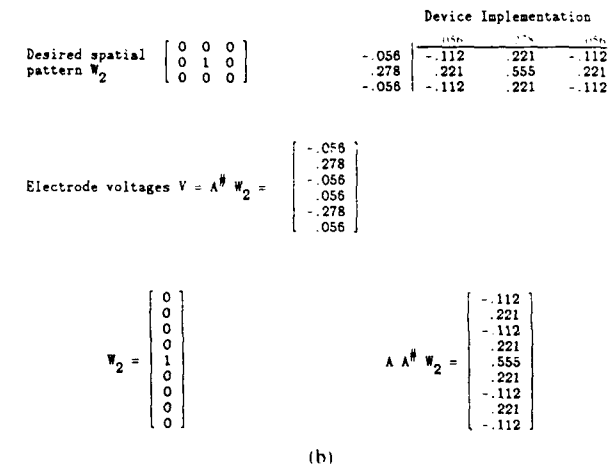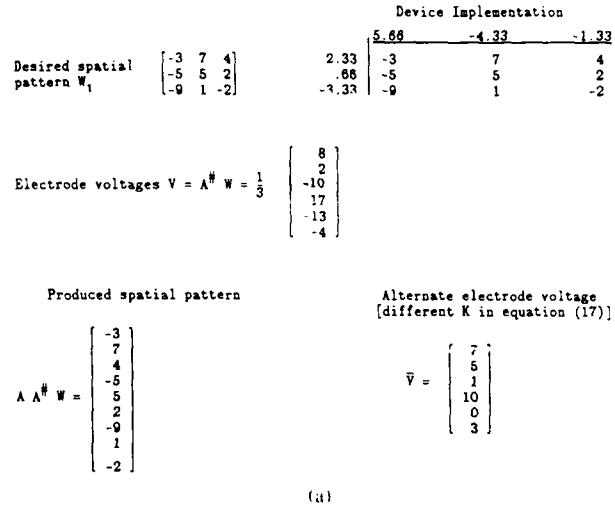
Fig. 2. Example of desired spatial patterns which can be reproduced (a) exactly (W_1) and (b) which cannot (W_2).
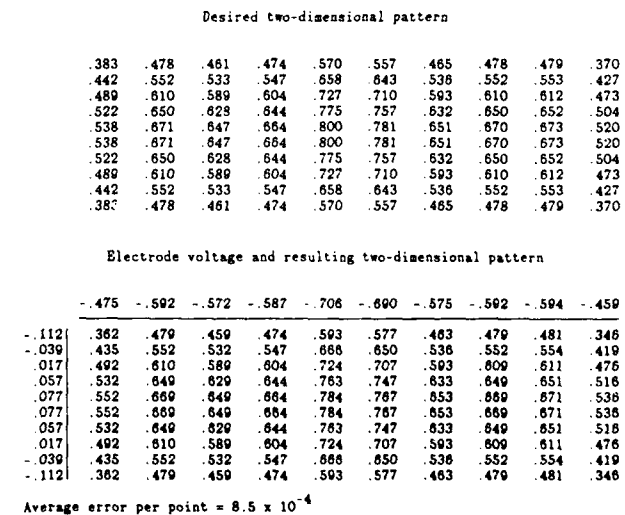
Fig. 3. Example of a desired 10×10 two-dimensional field and the crossed electrode structure reproduction.

The difference between the measured two-dimensional field from an edge-connected device and that measured by an array of independent elements can be visualized by contrasting the impulse response of the two devices. Consider a unit impulse

Desired two-dimensional pattern

.319	.495	.291	.198	.570	.525	.104	.367	.499	.264
.369	.572	.335	.229	.658	.806	.121	.424	.577	.306
.408	.632	.371	.253	.727	.670	.133	.468	.638	.338
.435	.674	.395	.270	.775	.714	.142	.499	.680	.361
.449	.695	.407	.278	.800	.737	.147	.515	.701	.372
.449	.695	.407	.278	.800	.737	.147	.515	.701	.372
.435	.674	.395	.270	.775	.714	.142	.499	.680	.361
.408	.632	.371	.253	.727	.670	.133	.468	.638	.338
.369	.572	.335	.229	.658	.806	.121	.424	.577	.306
.319	.495	.291	.198	.570	.525	.104	.367	.499	.264

Electrode voltage and resulting two-dimensional pattern

	-.396	-.613	-.360	-.246	-.706	-.650	-.129	-.454	-.619	-.328
-.086	.309	.527	.273	.159	.619	.564	.042	.367	.532	.242
-.030	.366	.583	.329	.215	.675	.620	.099	.424	.588	.298
.013	.410	.627	.373	.259	.720	.664	.143	.468	.633	.342
.044	.440	.658	.404	.290	.750	.695	.174	.499	.663	.373
.059	.456	.673	.420	.305	.766	.710	.189	.514	.679	.388
.059	.456	.673	.420	.305	.766	.710	.189	.514	.679	.388
.044	.440	.658	.404	.290	.750	.695	.174	.499	.663	.373
.013	.410	.627	.373	.259	.720	.664	.143	.468	.633	.342
-.030	.366	.583	.329	.215	.675	.620	.099	.424	.588	.298
-.086	.309	.527	.273	.159	.619	.564	.042	.367	.532	.242

Average error per point = 2.15×10^{-3}

Fig. 4. Example of a desired 10×10 two-dimensional field with higher spatial frequency content than Fig. 3, and the crossed-electrode structure reproduction.

P_i applied to one of the elements of each array. The voltage produced by a square edge-connected array ($2N$ elements) will be given by reciprocity to be ($K = 0$)

$$V = \frac{1}{N} A^T + \left| \frac{1}{2N^2} G \right| P_i \qquad (20)$$

nonsquare geometries follow similarly. The apparent measured two-dimensional field will be

$$P_m = AV \left| \frac{1}{N} AA^T + \frac{1}{2N^2} AG \right| P_i \qquad (21)$$

so that the operator in brackets will modify the actual field. This effect is seen clearly in Fig. 2(b) for a 3×3 device. As can be seen, the edge-connected array produces a cyclic impulse response. The effect of this impulse response on the power spectral density and beamforming effectiveness will be calculated in the next section.

To employ the edge-connected array in beamforming, one may first produce the apparent 2D field

$$P(t) = \frac{1}{N} AV(t). \qquad (22)$$

This would be the measured image when the device is employed in an image mode. The 2D field here is ordered lexicographically as

$$P(t) = \begin{bmatrix} P_{11}(t) \\ P_{12}(t) \\ \vdots \\ P_{1N}(t) \\ P_{2N}(t) \\ \vdots \\ P_{NN}(t) \end{bmatrix}$$

and beamforming is accomplished as

$$B = \sum s_i P_i(t + \tau_i) = \frac{1}{N} \sum_{i=0}^{N-1} \sum_{j=0}^{2N-1} A_{ij} V_j(t + \tau_i) s \qquad (23)$$

where s_j is a two-dimensional weighting pattern which may be employed. This is determined *a priori* and may be unity. Thus to use an edge-connected array, one extra step (the sum over j) must be carried out. If it is recalled that this matrix multiplication is simply subtraction of the column voltages from the row (relative to some arbitrary but fixed ground), this added step is seen to be trivial and can lessen the storage required to represent the field. This added processing is the price for the increased number of sensing elements while retaining only $2N$ measurements and clearly demonstrates the tradeoff between added processing complexity (edge-connected array) and implementation and construction complexity (independent element array).

ANALYSIS—BEAMFORMING TRANSFER FUNCTION

Consider the geometry shown in Fig. 5. We will analyze this structure with the following assumptions [13]-[15]:

1) the transducer possesses 2 orthogonal principal axes;
2) separations between centers of successive transducer elements lying in the direction of a principal axis are equal;
3) time delays between successive transducers elements lying in the direction of a principal axis are equal;
4) the temporal response of each active segment is identical for all segments of the array and is specified by the power spectral density $|F(\omega)|^2$;
5) the spatial response of each active segment is identical for all segments of the array and is specified by the power spectral density $M(k_n, k_p)$.

For the geometry of Fig. 5

$$M(k_n, k_p) = \frac{\sin^2 \frac{k_n b}{2} \sin^2 \frac{k_p l}{2}}{\left| \frac{k_n b}{2} \right|^2 \left| \frac{k_p l}{2} \right|^2}. \qquad (24)$$

Given the assumptions above, it has been shown that the receiver transfer function is

$$W(k, \omega) = 8\pi^3 |F(\omega)|^2 M(k_n, k_p) \left| \sum_j \sum_m \exp\left[-ik \cdot (y_j - y_m) \right. \right.$$
$$\left. \left. - i\omega(\tau_j - \tau_m) \right] \cdot s_j s_m \right|^2, \qquad i = \sqrt{-1} \qquad (25)$$

where y_j is the position of the jth active segment, τ_j is the time delay applied to the output of this segment, and s_j the relative sensitivity. This then can be written

$$W(k, \omega) = 8\pi^3 |F(\omega)|^2 M(k_n, k_p) \sum_{j=0}^{N-1} \sum_{m=0}^{P-1}$$
$$\cdot \exp - i(jk_n d + mk_p e + j\omega\tau_n + m\omega\tau_p) s_j s_m^2. \qquad (26)$$

This may be extended to include a more general case than the case where each active element is independent, by rewriting (26) as ($\tau' = \omega\tau$)

$$W(k, \tau') = 8\pi^3 |F(\omega)|^2 M(k_n k_p) |S(k_n, k_p, \tau')|^2 \qquad (27)$$

$$S(k_n, k_p, \tau') = \sum_{j=0}^{N-1} \sum_{m=0}^{P-1} e^{-i(j\omega\tau_n + m\omega\tau_p)} s_j s_m$$

$$\cdot \sum_{g=0}^{N-1} \sum_{h=0}^{P-1} I_{jgmh} e^{-i(gk_n d + hk_p e)} \qquad (28)$$
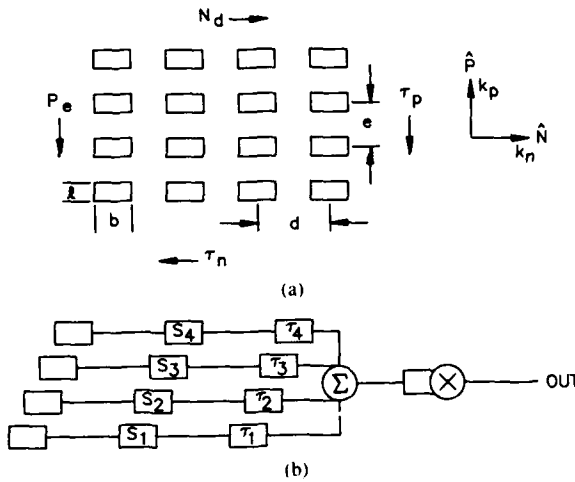
Fig. 5. Array geometry with (a) parameter definitions and (b) conventional beamforming implementation.

Independent Elements	Edge-Connected Array
$\begin{bmatrix} 0 & 0 & 0 \\ 0 & 1 & 0 \\ 0 & 0 & 0 \end{bmatrix}$	$\begin{bmatrix} -.112 & .221 & -.112 \\ .221 & .555 & .221 \\ -.112 & .221 & .112 \end{bmatrix}$

Results of Unit Response
Applied to Center

$\begin{bmatrix} 1 & 0 & 0 \\ 0 & 0 & 0 \\ 0 & 0 & 0 \end{bmatrix}$	$\begin{bmatrix} .555 & .221 & .221 \\ .221 & -.112 & -.112 \\ .221 & -.112 & -.112 \end{bmatrix}$

Results of Unit Response
Supplied to Upper Left Element

Fig. 6. Cyclic impulse response of crossed-electrode geometry.

where I_{jgmh} is the impulse of the structure. For the case of independent active elements, I_{jgmh} is simply a Kronecker delta function, i.e., each element responds to a point pressure input at only the active element to which it is applied. Then for the previous case [13]–[15]

$$I_{jgmh} = \delta_{jg}\delta_{mh} \quad \text{where } \delta_{jg} = 1 \quad \text{if } j = g$$
$$= 0 \quad \text{otherwise} \quad (29)$$

it was shown for $s_i = 1$[13]

$$S(k_n, k_p, \tau') = \sum_{j=0}^{N-1}\sum_{m=0}^{P-1} \exp -i[j(k_n d + \omega\tau_n)$$
$$+ m(k_p e + \omega\tau_p)]$$
$$= \frac{1 - e^{-iN(k_n d + \omega\tau_n)}}{1 - e^{-i(k_n d + \omega\tau_n)}} \frac{1 - e^{-iP(k_p e + \omega\tau_p)}}{1 - e^{-i(k_p e + \omega\tau_p)}} \quad (30)$$

so that

$$|S(k_n, k_p, \tau')|^2$$
$$= \frac{\sin^2 N\left|\dfrac{k_n d + \omega\tau_n}{2}\right| \sin^2 P\left|\dfrac{k_p e + \omega\tau_p}{2}\right|}{\sin^2\left|\dfrac{k_n d + \omega\tau_n}{2}\right| \sin^2\left|\dfrac{k_p e + \omega\tau_p}{2}\right|}. \quad (31)$$

For the case of the edge-connected array, the impulse response may be found to be (17)

$$I_{jgmh} = \frac{1}{P}\delta_{jg} + \frac{1}{N}\delta_{mh} - \frac{1}{NP}. \quad (32)$$

This is a cyclic convolutional impulse response and can be contrasted with that of the independent elements as shown in Fig. 6.

In this case, (28) takes the form

$$S_c(k_n, k_p, \tau')$$
$$= \sum_{j=0}^{N-1}\sum_{m=0}^{P-1} e^{-i\omega(j\tau_n + m\tau_p)} s_j s_m \left[\frac{1}{P}e^{-ijk_n d}\sum_{h=0}^{P-1} e^{ihk_p e} \right.$$
$$\left. + \frac{1}{N}e^{-imk_p e}\sum_{g=0}^{N-1} e^{igk_n d} - \frac{1}{NP}\sum_{g=0}^{N-1}\sum_{h=0}^{P-1} e^{-i(gk_n d + hk_p e)} \right] \quad (33)$$

$$S_c(k_n, k_p, \tau')$$
$$= \sum_{j=0}^{N-1}\sum_{m=0}^{P-1} e^{-i\omega(j\tau_n + m\tau_p)} s_j s_m \left[\frac{1}{P}e^{-ijk_n d}\frac{1 - e^{-iPk_p e}}{1 - e^{-ik_p e}} \right.$$
$$\left. + \frac{1}{N}e^{-imk_p e}\frac{1 - e^{-iNk_n d}}{1 - e^{-ik_n d}} - \frac{1}{NP}\frac{1 - e^{-iNk_n d}}{1 - e^{-ik_n d}}\frac{1 - e^{-iPk_p e}}{1 - e^{-ik_p e}} \right] \quad (34)$$

for $s = 1$ (34) reduces to

$$S_c(k_n, k_p, \tau')$$
$$= \frac{1}{P}\frac{1 - e^{-iN(k_n d + \omega\tau_n)}}{1 - e^{-i(k_n d + \omega\tau_n)}}\frac{1 - e^{-iP\omega\tau_p}}{1 - e^{-i\omega\tau_p}}\frac{1 - e^{iPk_p e}}{1 - e^{k_p e}}$$
$$+ \frac{1}{N}\frac{1 - e^{-iP(k_p e + \omega\tau_p)}}{1 - e^{-i(k_p e + \omega\tau_p)}}\frac{1 - e^{-iN\omega\tau_n}}{1 - e^{-i\omega\tau_n}}\frac{1 - e^{-iNk_n d}}{1 - e^{-ik_n d}}$$
$$- \frac{1}{NP}\frac{1 - e^{-iN\omega\tau_n}}{1 - e^{-i\omega\tau_n}}\frac{1 - e^{-iNk_n d}}{1 - e^{-ik_n d}}\frac{1 - e^{-iP\omega\tau_p}}{1 - e^{-i\omega\tau_p}}\frac{1 - e^{iPk_p e}}{1 - e^{k_p e}} \quad (35)$$

$$S_c(k_n, k_p, \tau_n', 0)$$
$$= \frac{1 - e^{-iN(k_n d + \omega\tau_n)}}{1 - e^{-i(k_n d + \omega\tau_n)}}\frac{1 - e^{-iPk_p e}}{1 - e^{-ik_p e}}$$
$$+ \frac{1}{N}\frac{1 - e^{iPk_p e}}{1 - e^{ik_p e}}\frac{1 - e^{-iN\omega\tau_n}}{1 - e^{-i\omega\tau_n}}\frac{1 - e^{-iNk_n d}}{1 - e^{-ik_n d}}$$
$$- \frac{1}{N}\frac{1 - e^{-iN\omega\tau_n}}{1 - e^{-i\omega\tau_n}}\frac{1 - e^{-iNk_n d}}{1 - e^{ik_n d}}\frac{1 - e^{-iPk_p e}}{1 - e^{-ik_p e}}. \quad (36)$$

The last two terms cancel leaving

$$S_c(k_n, k_p, \tau_n', 0) = \frac{1 - e^{-iN(k_n d + \omega\tau_n)}}{1 - e^{-i(k_n d + \omega\tau_n)}}\frac{1 - e^{-iPk_p e}}{1 - e^{-ik_p e}} \quad (37)$$

similarly

$$S_c(k_n, k_p, 0, \tau_p') = \frac{1 - e^{-iP(k_p e + \omega\tau_p)}}{1 - e^{-i(k_p e + \omega\tau_p)}}\frac{1 - e^{-iNk_n d}}{1 - e^{-ik_n d}} \quad (38)$$

so that

$$\frac{S_c(k_n, k_p, \tau_n', 0)S_c(k_n, k_p, 0, \tau_p')}{S_c(k_n, k_p, 0, 0)}$$
$$= \frac{1 - e^{-iN(k_n d + \omega\tau_n)}}{1 - e^{-i(k_n d + \omega\tau_n)}}\frac{1 - e^{-iP(k_p e + \omega\tau_p)}}{1 - e^{-i(k_p e + \omega\tau_p)}} \quad (39)$$

which is identical to $S(k_n, k_p, \tau_n', \tau_p')$ of (30).

The easiest way to visualize the process is to analyze a spe-
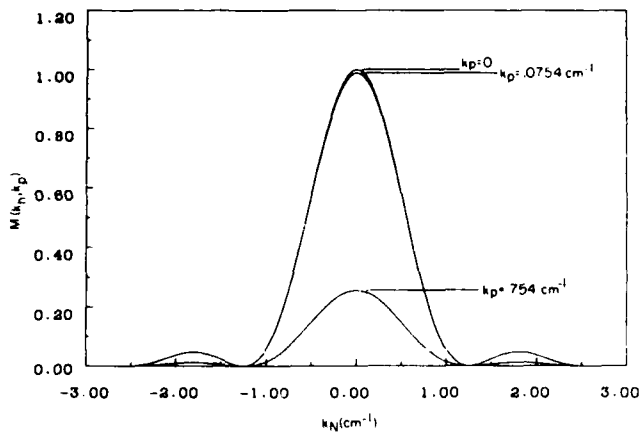
Fig. 7. Single-element (rectangular) spatial frequency transfer function for parameters given in text.
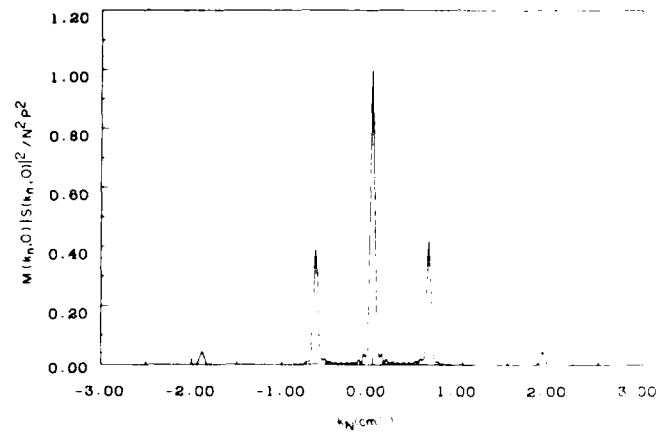
Fig. 8. Normalized transfer function for no time delay $\tau'_n = \tau'_p = 0$ along the $k_p = 0$ axis. Both the conventional and crossed-electrode geometries provide the same results. $N = P = 10$.

cific geometry. Consider the case (dimensions in centimeters)

$$N = 10$$

$$P = 10$$

$$d = 10$$

$$e = 10$$

$$b = 5$$

$$l = 5.$$

Fig. 7 displays the single element transfer function $M(k_n, k_p)$ along several k_p axes. Fig. 8 shows the product $M(k_n, k_p) | S(k_n, k_p, \tau')|^2/N^2 P^2$ along the $k_p = 0$ axis for the above example ($\tau'_n = \tau'_p = 0$). The results of the edge-connected array are the same for this case. The effect of changing N and P may be seen by comparing a similar calculation for $N = P = 3$ in Fig. 9. The effect of a single time delay are seen in Figs. 10 and 11 which displays the product $M | S |^2/N^2 P^2$ along the $k_p = 0$ axis for the time delays $(\tau'_n, \tau'_p) = (1.57, 0)$ and $(5.0, 0)$. For this case, the peak in the (k_n, k_p) plane moves from $(0, 0)$ to $(-0.157, 0)$ and $(-0.5, 0)$ as expected. In the latter case, a second lobe has come into the region of the function M to appear similar to the main lobe in Fig. 8 for no time delay. Fig. 12 shows the product $M | S |^2/N^2 P^2$ along the $k_n = 0$ axis for a time delay of $(\tau'_n, \tau'_p) = (0, 1.57)$ which appears like Fig. 10 by symmetry. Fig. 13 displays a time delay $(\tau'_n, \tau'_p) = (1.57, 1.57)$ along the $k_p = -0.151$ axis (near the peak) for the independent element array. As expected, the peak moved to $(-0.157, -0.157)$. Fig. 14 displays a similar calculation for the edge-connected array. It can be seen that the lobes have split into two sets of components, one contribution remaining at the origin, the other smaller one moving to the expected position. Thus, applying time delays simultaneously along both axes will result in a transfer function which is different than a similar operation on an independent element array, i.e., $S(k_n, k_p, \tau_n, \tau_p) \neq S_e(k_n, k_p, \tau_n, \tau_p)$. However, as shown by Figs. 10, 12–14 and (27) and (39), if time delays are applied along a single axis (normalized by zero time delay) and the results are multiplied by a time delay of the orthogonal axis, the resulting transfer function will be the same as the independent element case. This is easily seen in our example since (Fig. 13 and (31)) $S(k_n, -0.157, 1.57, 1.57) = S(k_n, 0, 1.57, 0)$. The more general case is also true as shown by (39). The edge-connected array must be operated in a two-step product mode where each step
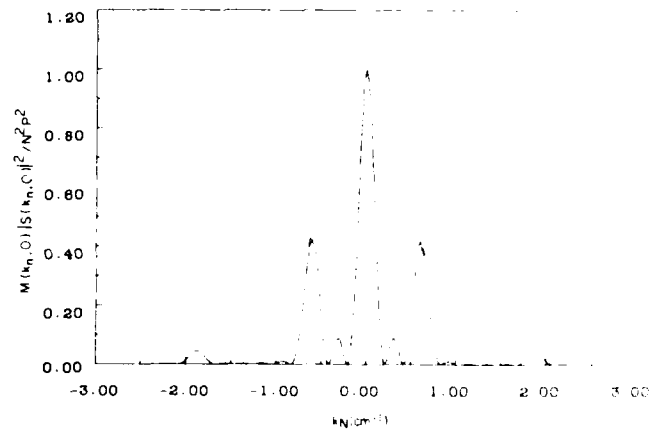
Fig. 9. Effect of reducing the number of elements from $N = P = 10$ (Fig. 8) to $N = P = 3$. Note the broadening of the lobes. $\tau'_n = \tau'_p = 0$.
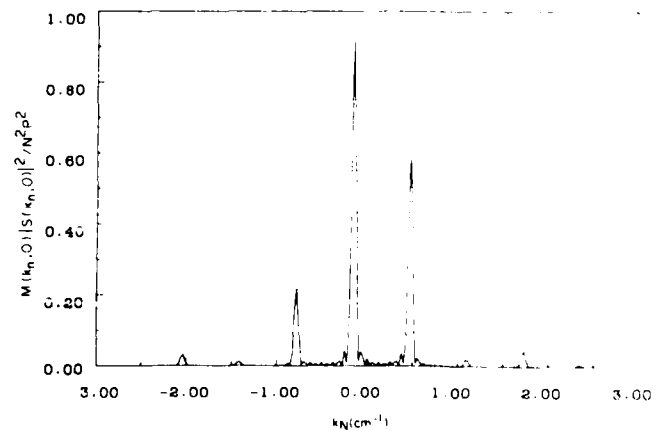
Fig. 10. Normalized transfer function along the $k_p = 0$ axis for time delay $\tau'_n = 1.57$. Note how the main lobe has been swept away from the origin as expected. This result is identical for both the conventional independent element array and the crossed-electrode array. $\tau'_p = 0$, $N = P = 10$.

beamforms along a single axis. The results of this process will be identical to an independent element array.

As an aid in visualizing the operational characteristics of a system with a specified number of processing channels, consider Figs. 15 and 16. The assumption is that a system which
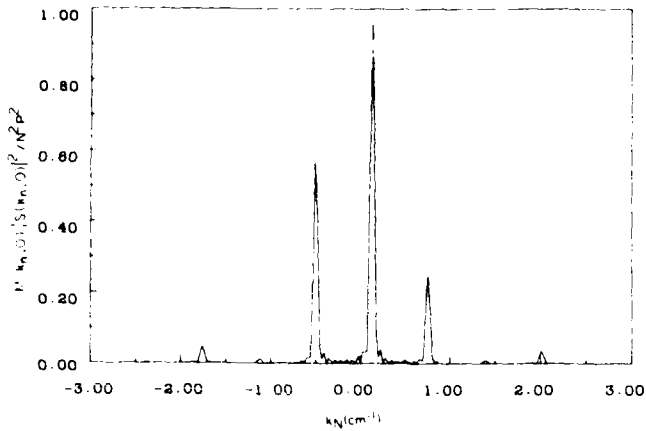
Fig. 11. Results similar to Fig. 10 for time delay $\tau_n' = 5.0$. Note the main lobe has moved further to the left and a second lobe has entered from the right to the right of the origin. $\tau_p' = 0$, $N = P = 0$.
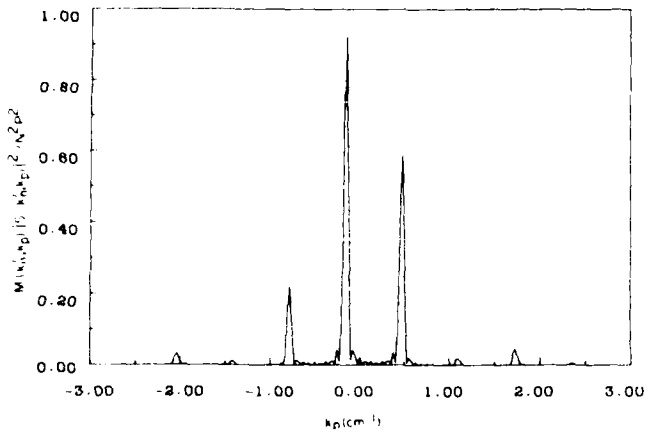
Fig. 12. Normalized transfer function for the conventional and crossed-electrode geometries along the $k_n = 0$ axis for a time delay $\tau_p' = 1.51$, $\tau_n' = 0$, $N = P = 0$.
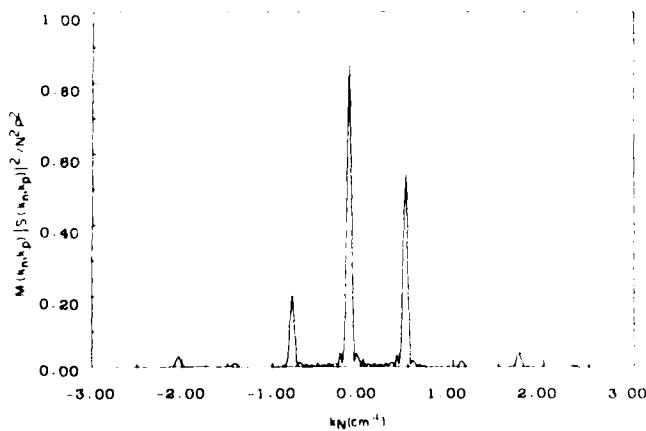
Fig. 13. Normalized transfer function for the conventional geometry for the time delay $\tau_n' = \tau_p' = 1.51$ along the $k_p = -0.151$ cm^{-1} axis. The main lobe has been swept to the left of the origin as expected from Figs. 12 and 10. $N = P = 0$.

can process 16 channels of data exists ($d = e = 10$, $b = l = 5$ as before), for the independent element case this results in a 4 × 4 array, Fig. 15, whereas the edge-connected case has 8 connections on a side or 16 total and 64 interconnected sensing
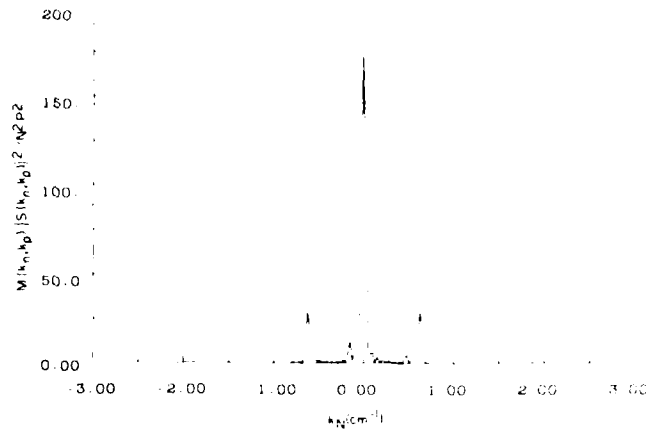
Fig. 14. Normalized transfer function for crossed-electrode geometry for the time delay $\tau_n' = \tau_p' = 1.57$ along the $k_p = -0.151$ cm^{-1} axis. Note that the lobe has split, one contribution remaining on the origin and a smaller one moving to the expected position. This indicates the beamforming can not be done in a one-step procedure with two time delays, but can be accomplished in two single time delay processes as shown in Figs. 10 and 12. $N = P = 0$.
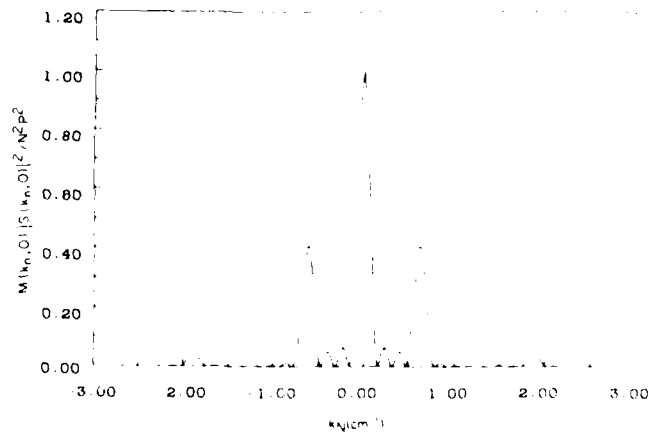
Fig. 15. Normalized transfer function for a hypothetical system with capacity for 16 inputs. A conventional system would have 16 elements (4 × 4) individually addressed. $\tau_n' = \tau_p' = 0$, $N = P = 4$.
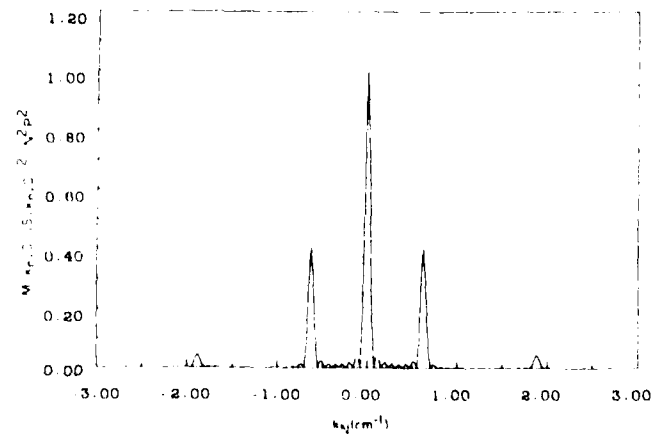
Fig. 16. Identical assumptions as Fig. 15 for the cross-electrode geometry which would have 8 elements on a side. Note the reduced width of the lobes. $\tau_n' = \tau_p' = 0$, $N = P = 8$.

areas. The pattern $M|S|^2/N^2P^2$ displayed for $(\tau_n', \tau_p') = (0, 0)$ displays the superior resolving power of the edge-connected array.

CONCLUSION

The concept of a crossed-electrode edge-coupled array has been introduced and shown to have several significant advantages over conventionally addressed two-dimensional structures. Specifically this geometry requires only $2N$ electrode leads as opposed to N^2 for an $N \times N$ device. While this structure requires an additional signal processing step for applications such as beamforming, this will in many instances be acceptable since the cost of signal processing is decreasing with time.

As a projector, the device is shown to be capable of replicating two-dimensional fields which have most of their energy located near the spatial frequency axis. As energy moves to higher frequency, particularly away from either axis (spatial frequency axis corresponding to the top electrode direction or bottom electrode direction), the device suffers more error. There are many applications, however, which fall within this constraint, particularly those which would gain from the addition of more active areas at the expense of a limited performance degradation.

The analysis concerned with employing this geometry in a beamforming mode shows no performance degradation provided an extra signal processing step is included. This is an attractive tradeoff for many applications since signal processing costs are continually being lowered. This analysis does not concern itself with the implementation of beamformer signal processing hardware, but the observation that no performance degradation occurs if a two-step process is used (rather than the conventional single step) should make this geometry attractive for further consideration in beamforming and tracking applications.

REFERENCES

[1] J. L. Lumley, *Stochastic Tools in Turbulence.* New York: Academic, pp. 54–58, 1970.
[2] M. Loeve, *Probability Theory II,* 4th ed. New York: Springer, pp. 143–151, 1978.
[3] W. D. Ray and R. M. Driver, "Further decomposition of the Karhunen–Loeve series representation of a stationary random process," *IEEE Trans. Inform. Theory,* vol. IT-16, pp. 663–667, 1970.
[4] A. K. Jain, "A fast Karhunen–Loeve transform for a class of random processes," *IEEE Trans. Commun.,* vol. COM-24, pp. 1023–1029, 1976.
[5] H. C. Andrews and B. R. Hunt, *Digital Image Restoration.* Englewood Cliffs, NJ: Prentice-Hall, vol. 85, 1977.
[6] R. Penrose, "A generalized inverse for matrices," *Proc. Cambridge Phil. Soc.,* vol. 51, pp. 406–413, 1955.
[7] N. S. Urquehart, "Computation of generalized inverse matrices which satisfy specified conditions," *SIAM Rev.,* vol. 10, pp. 216–218, 1968.
[8] G. Meier, E. Sackmann, and J. G. Grabmauer, *Applications of Liquid Crystals.* New York, Springer: pp. 12, 134, 153–155, 1975.
[9] W. Blake, *Mechanics of Flow-Induced Sound and Vibration,* vol. 2. New York: Academic, 1980.
[10] R. Kennedy, "Cancellation of turbulent boundary-layer pressure fluctuations," *J. Acoust. Soc. Amer.,* vol. 57, pp. 1062–1066, 1975.
[11] W. K. Blake and D. M. Chase, "Wavenumber-frequency spectra of turbulent-boundary-layer pressure measured by microphone arrays," *J. Acoust. Soc. Amer.,* vol. 49, pp. 862–877, 1971.
[12] Y. F. Hwang and F. E. Geib, "Estimation of the wavevector-frequency spectrum of turbulent boundary layer wale pressure by multiple linear regression," *JYASRD,* vol. 106, pp. 334–342, 1984.
[13] G. Maidanik, "Flush-mounted pressure transducer systems as spatial and spectral filters," *J. Acoust. Soc. Amer.,* vol. 42, pp. 1017–1024, 1967.
[14] G. Maidanik and D. W. Jorgensen, "Boundary wave-vector filters for the study of the pressure field in a turbulent boundary layer," *J. Acoust. Soc. Amer.,* vol. 42, pp. 494–501, 1967.
[15] M. Born and E. Wolf, *Principles of Optics.* New York: Pergamon, pp. 401–402, 1959.

Harvey C. Schau ~~~~~~~~~~~~~~~ He received the B.S. and M.S. degrees in physics from Florida Atlantic University in 1972 and 1973, respectively, and the Ph.D. degree in engineering science from the University of Florida in 1975.

From 1975 until the present he has worked in both the aerospace industry and government laboratories. From 1983 until 1988 he was a Research Physicist with the Naval Research Laboratory. His research interests are applying signal processing and systems engineering to problems in optics and acoustics, particularly remote sensing, target recognition, and system characterization methodology.